ACS APPLIED MATERIALS & INTERFACES

RESEARCH ARTICLE

www.acsami.org

Mixed Alkylsilane Functionalized Surfaces for Simultaneous Wetting and Homeotropic Anchoring of Liquid Crystals

Patrick S. Noonan,[†] Amit Shavit,[†] Bharat R. Acharya,[‡] and Daniel K. Schwartz*[,†]

[†]Department of Chemical and Biological Engineering, University of Colorado, Boulder,Colorado 80309-0424, United States

[‡]Platypus Technologies LLC, 5520 Novel Drive, Suite 100, Madison, Wisconsin 53711, United States

Supporting Information

ABSTRACT:

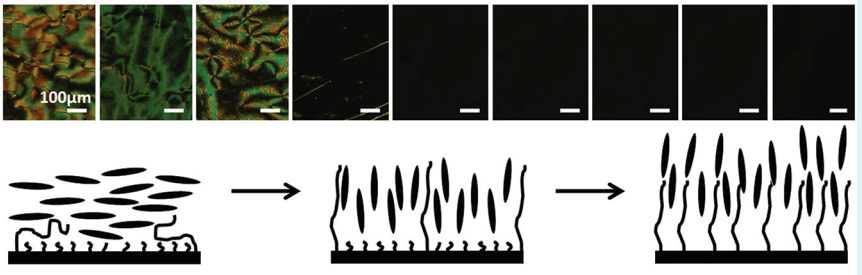

Surfaces functionalized with a self-assembled monolayer (SAM) formed from a mixture of two alkylsilanes with different chain lengths have been designed to simultaneously improve the liquid crystal (LC) wettability and promote homeotropic anchoring of the LC. Most chemically functionalized surfaces (e.g., long alkyl chain SAMs) that promote homeotropic alignment of LC possess low surface energy and result in poor LC wettability, inhibiting LC infiltration into microstructured surfaces and sometimes resulting in LC dewetting from the surface. However, a surface modified with a mixed SAM of octadecyltriethoxysilane (C18) and ethyltriethoxysilane (C2) exhibited very low LC contact angle while providing homeotropic anchoring. Ellipsometry was used to correlate the bulk concentration of C18 in the deposition solution to the surface coverage of C18 in the mixed monolayer; these bulk and surface concentrations were found to be equal within experimental uncertainty. The LC contact angle was found to depend nonmonotically with the surface coverage density, with a minimum ($14.4 \pm 0.1°$) at a C18 surface coverage of 0.26 ± 0.08. Homeotropic LC anchoring was achieved at a C18 surface coverage of $\geq 0.11 \pm 0.04$, in the regime where a minimum in the LC contact angle was observed. The practical application of this approach to surface modification was demonstrated using a micropillar array sensor substrate. When the array was functionalized with a conventional C18 SAM, the LC did not infiltrate the array and exhibited a contact angle of $47.4 \pm 0.5°$. However, the LC material successfully infiltrated and wetted the same microstructured substrate when functionalized with a C18/C2 mixed SAM, while still exhibiting the desired homeotropic anchoring.

KEYWORDS: liquid crystals, self-assembled monolayer, contact angle, surface coverage, mixed monolayer, wetting

INTRODUCTION

Liquid crystal (LC)-based sensors show promise in many applications, including the detection of infectious disease biomarkers,[1−3] environmental pollutants,[1,4,5] harmful gases,[1,4−6] and protein reactions.[7] For LC sensors to function properly, a number of critical parameters must be carefully controlled, including the LC film thickness, the LC orientation, and substrate surface energy. In typical LC display applications, the LC film thickness is determined by the spacing between two solid surfaces. In sensors, however, the LC film is often supported on a single substrate and is in contact with a vapor or liquid phase that contains the target or analyte species. Therefore, the LC film thickness is more difficult to control. In many cases, this control is achieved by containing the LC within a microstructured environment where capillary interactions can be exploited to maintain a uniform and stable film. A simple example of this, appropriate for prototype applications, involves an electron microscopy grid.[8] The holes within such a grid can be filled with LC, and to a first approximation, the LC layers adopt a thickness equal to the height of the grid. A more robust and reproducible approach involves stabilizing a continuous LC film in a microstructured environment, e.g., an array of cylindrical micropillars on a glass substrate.[5,9] In this scenario, an LC material infiltrates the entire array, filling the space between the micropillars, and capillary forces stabilize the LC film at a thickness equal to the height of the micropillars.

In virtually all LC applications, a specific LC orientation must be defined at one or more interfaces. Examples include homeotropic anchoring, where the long axes of the LC molecules are

Received: August 2, 2011
Accepted: September 26, 2011
Published: October 17, 2011

oriented in the surface normal direction, or planar anchoring, where the LC long axes lie in the surface plane. A number of standard surface modification approaches have been developed and are used to control LC surface anchoring on planar surfaces for various applications.[10−14] Microstructured substrates used for sensor applications need to fulfill an additional requirement, however, because the LC material must infiltrate the substrate, maintain a uniform thickness, and remain stable. In particular, if the balance of interfacial free energies is such that the contact angle of the LC on the alignment layer is too large, the LC material may not spontaneously infiltrate the microstructured environment or it may dewet during use. Thus, there is a need for chemical functionalization technologies that can be used to modify the surfaces of microstructured environments and that spontaneously promote LC wetting of these environments.

It is often desirable to maintain homeotropic LC orientation at a solid−LC interface for sensor applications.[3,7,8,15] On a conventional planar glass surface, this is typically achieved using surfaces functionalized with a self-assembled monolayer (SAM) composed of long chain alkylsilanes.[11,13] The deposition of an alkylsilane SAM involves spontaneous adsorption from a liquid or vapor phase and an assembly driven by island growth,[16,17] that is stabilized by covalent Si−O−Si linkages among silane moieties as well as between silane moieties and surface silanol groups.[18,19] These SAM alignment layers are convenient and appropriate for many LC sensor substrates. However, surfaces functionalized with long chain alkylsilane SAMs possess low surface energy and LC materials (and hydrocarbon liquids in general) typically exhibit moderately high contact angles, making these surfaces inappropriate to support a uniform LC film.

The relationship between LC alignment and the wettability of various monolayer compositions has been extensively studied.[10,11,20−22] Historically, a relationship was proposed that allowed one to predict the orientation of liquid crystals on a given substrate based on the governing relationship that homeotropic LC orientation can be achieved only on substrates where the LC surface tension (γ_{LC}) is greater than a critical surface tension of the substrate (γ_C) (i.e., high contact angle).[11,22] Such a relationship suggests that it would be difficult, if not impossible, to design surfaces that both are wettable by the LC and also induce homeotropic anchoring. Despite reports that directly confirm this relationship,[22] others have shown that it is not universal.[20,21] Exceptions to the "rule" often involve situations where strong local directional interactions are dominant. For example, carboxylic acid terminated SAMs functionalized with certain metal salts promote homeotropic orientation and a low LC contact angle of nitrile-containing LCs.[9,23] In this case, the homeotropic orientation is attributed to a specific coordination interaction between the nitrile group of the LC and the metal center. Another example involves glass surfaces functionalized with amine-terminated SAMs. Despite the fact that they exhibit increased γ_C over other substrates (e.g., functionalized with long chain alkyl silanes)[24] typically used for homeotropic alignment, amine-terminated SAMs are used to induce homeotropic LC alignment,[6,12,14,15] apparently due to strong localized dipole−dipole interactions between the polar LC molecules and the surface amine.[12] Low LC contact angles have not been reported, however, on amine-terminated glass surfaces.

To date, these specialized examples of LC alignment layers that induce high homeotropic anchoring energy and a low LC contact angle have only been prepared via thiol chemistry on metal surfaces. We were unable to find a published example of a surface functionalization strategy that can be applied to an oxide material, using silane chemistry. In fact, most high energy surfaces possessing low LC contact angles have been found to yield low pretilt angles,[10,11,25,26] i.e., promote planar or tilted LC alignment.

LC alignment on oxide surfaces functionalized with silanes is of significant technological importance, not only for LC sensor applications but also in the display industry. The utilization of functionalized oxides (e.g., glass, indium tin oxide) allows for improved transmittance over metal surfaces (e.g., gold), which is relevant in the design of LC displays. Metal substrates also require additional processing steps to deposit a thin metal film onto a supporting substrate,[5,23] while oxide substrates can be functionalized using simple deposition procedures.[13] Furthermore, LC sensor applications may be sensitive to the presence of ions,[3] and the use of an oxide substrate, over a metallic substrate, can reduce the risk of ionic contamination affecting the sensor response. Therefore, our aim was to develop a SAM that promotes homeotropic anchoring and LC wetting on a functionalized oxide substrate via silane chemistry.

Studies have suggested that homeotropic anchoring can sometimes be achieved by less than complete coverage of long alkyl chains.[3,27,28] We postulated, therefore, that high energy (i.e., LC wettable) surfaces, promoting homeotropic alignment, might be achieved by functionalizing surfaces with mixed SAMs where the surface density of long chains was diminished via mixing with a second component that would serve to reduce the LC contact angle. This strategy allows for the design of SAMs with simple surface chemistry to achieve tunable surface properties. In this report, results from a systematic study of various mixtures of long and short chain alkylsilanes are presented.

MATERIALS AND METHODS

Mixed Monolayer Deposition. Self-assembled monolayers of alkylsilanes were prepared according to published procedures[13] modified for mixed monolayers. Soda lime glass microscope slides (Corning Inc.) were cleaned sequentially with 2% aqueous micro-90, deionized water (18.2 MΩ), and piranha solution [30% aqueous H_2O_2 (Fisher Scientific) and concentrated H_2SO_4 (Fisher Scientific) 1:3, v/v] at 80 °C for 1 h. (Warning: piranha solution reacts strongly with organic compounds and should be handled with extreme caution; do not store in closed container.) After piranha cleaning, the microscope slides were rinsed with deionized water and dried under a stream of ultrapure N_2. A deposition solution of *n*-butylamine (Fisher Scientific) and alkylsilanes was prepared in toluene (Fisher Scientific) at 1:3:200 volumetric ratio, respectively. The alkylsilanes, octadecyltriethoxysilane (C18), and ethyltriethoxysilane (C2) (Gelest Inc.) were mixed at varying ratios (v_{C18}/v_{C2} = 0, 0.06, 0.11, 0.22, 0.33, 0.44, 0.66, 0.88, 1.00). The deposition solution was warmed to 60 °C; clean and dry microscope slides were first rinsed with toluene and then submerged in the warm deposition solution. The slides were incubated in the deposition solution for 1 h at 60 °C. Upon removal, the slides were rinsed with toluene, dried under a stream of ultrapure N_2, and stored at room temperature in a vacuum desiccator.

Contact Angle Measurements. Contact angles (θ_C) were measured on three substrates at three random locations, for each mole fraction of C18 tested, using the static sessile drop method with a custom-built contact angle goniometer. The variability between samples was found not to be significantly different from the variability within a given sample, and the error in the contact angle is reported as the standard error. Water contact angles were measured by adding a ~1 μL

drop of water to the surface dispensed from a syringe positioned directly above the surface. The drop was imaged immediately, to prevent evaporation, and imaging software (First Ten Angstroms, Inc.) was used to extract the contact angle for $\theta_C > 15°$. For $\theta_C < 15°$, ImageJ (NIH Freeware) was used to manually determine the contact angle due to poor fits from the image analysis software at these low contact angles. A LC mixture, E7 (a mixture of three cyanobiphenyls and a cyanoterphenyl, Merck KGaA), was used to measure the LC contact angle, and a hydrocarbon oil viscosity standard, N26 (a mixture of poly alpha olefins, Cannon Instrument Co.), was used to measure the contact angle of an isotropic oil. A micropipet (Eppendorf) was used to add a 0.2−0.5 μL drop of E7 or N26 onto the surface. The drop was imaged within 10 s of contact with the surface, and the contact angle was determined using imaging software ($\theta_C > 15°$) or ImageJ ($\theta_C < 15°$).

Polarized Light Microscopy. LC orientations on surfaces functionalized with different SAM compositions were determined by observing LC optical cells using an Olympus microscope (model BH2-UMA) modified for transmission mode. LC cells were prepared by pairing two identically functionalized surfaces facing each other to form a ∼5−10 μm thick cavity between them. The cavity was then filled with E7, via capillary action, in between two SAMs prepared from the same deposition solution. LC orientations were determined by imaging the optical cells between crossed polarizers. Homeotropic orientation was characterized by the lack of light transmission upon a complete 360° rotation of the sample, while birefringence due to tilted or planar LC orientation resulted in light transmission when the optical cell was imaged between crossed polarizers.

A microstructured substrate consisting of a hexagonal array (10 μm edge to edge spacing) of 5 μm tall cylindrical polymer micropillars (diameter D = 10 μm) on aluminum silicate glass was used to test the ability of E7 to spread on a micropillar array. While the use of different glass substrates for silane deposition has the potential to lead to a varying degree of SAM quality due to differences in the coverage of exposed hydroxyls, the use of appropriate sample preparation procedures (i.e., piranha, UV−ozone) results in a similar coverage of exposed hydroxyls and therefore SAM quality. SAMs were deposited onto two different samples of the micropillar array using two different deposition solutions (v_{C18}/v_{C2} = 1.0, 0.44), following a 1 h UV−ozone exposure. A 0.2 μL drop of E7 was added at the edge of the micropillars array and a combination of contact angle goniometry and polarized light microscopy was used to determine if the LC infiltrated the micropillars array and to characterize the LC anchoring if infiltration was successful.

Ellipsometry. A variable angle spectroscopic ellipsometer (J. A. Woollam Co., Inc.) was used to measure the thickness of the SAMs under study. A mixed monolayer was deposited onto silicon (100) wafers (WRS Materials) at varying ratios of C18 according to a procedure modified from that described above. The thickness of native SiO_2 (oxide) layer present on the silicon wafer was measured directly after the piranha cleaning step for each sample. Due to the time required for measurement of the oxide layer, there was a lag time between piranha cleaning and monolayer deposition of about 2 h, which can result in some contamination of the silicon wafers. To reduce the risk of contamination affecting the SAM deposition, the substrates were cleaned prior to SAM deposition using a 1 h UV−ozone exposure. For all measurements, the ellipsometry model assumed a 1 mm thick Si layer (n = 3.875−0.023i), and the change in phase (Δ) and amplitude (Ψ) at varying angles of incidence (60−80°, 5° increments) and wavelengths (500−900 nm, 100 nm increments) was measured to calculate the thickness of oxide and SAM assuming equal refractive indices (n = 1.46) for the SAM layer and the oxide layer. An average apparent oxide layer thickness taken across all the samples tested was measured (14.6 ± 0.4 Å) and was subtracted from measurements of the combined SAM and oxide layer to determine the SAM layer thickness. We note that contamination of the "clean" surfaces can result in an overestimate of the apparent silicon oxide layer thickness, affecting the absolute values of the SAM thickness. The relative thickness values of different SAMs, however, are relatively insensitive to these concerns. Uncertainties due to fitting of the ellipsometric model were consistently less than the experimental error due to variability within each sample, and the error in the film thickness is reported as the standard error due to variability between measurements (n = 3).

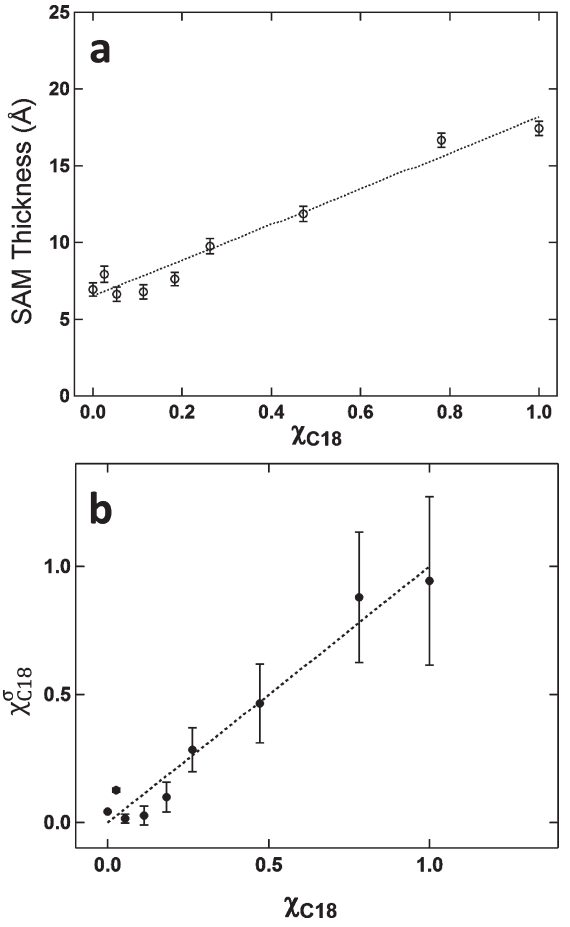

Figure 1. Mixed Monolayer Film Thickness: (a) Ellipsometric thickness of a C2/C18 mixed monolayer with varying χ_{C18}; (b) Calculated C18 surface coverage with varying χ_{C18}. The symbols represent experimental data, and the lines represent a fit to models described in the text.

Determination of Surface Fractions. The monolayer thickness is known to be very sensitive to deposition conditions,[18] leading to some inconsistency in the ellipsometric thicknesses reported in the literature.[18,19,29−31] Furthermore, the absolute thickness values are sensitive to errors in the determination of the silicon oxide layer and the specific choice of dielectric constants. Thus, these absolute thickness values determined by ellipsometry should be interpreted with care. The ellipsometric thicknesses for pure C2 and pure C18 monolayers prepared using the protocol described above was measured to be 7.0 ± 0.4 and 17.5 ± 0.4 Å, respectively (Figure 1a), in reasonable agreement with the values reported in the literature.[19] Importantly, since the monolayers were all prepared and characterized under the same conditions, these measurements allow the relative change in the monolayer thickness as a function of the mole fraction of C18 in the deposition solution (χ_{C18}) to be sufficient for deriving a relationship between the C18 surface coverage (χ^{σ}_{C18}) and χ_{C18}.

An expression was derived (see Supporting Information) relating χ^{σ}_{C18} to χ_{C18} from the measured film thickness, using a model involving

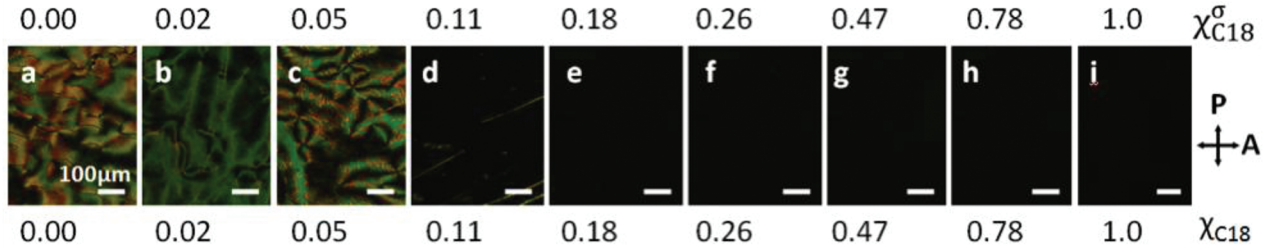

Figure 2. LC Anchoring Transition: Polarized microscopy images demonstrating the LC orientation at varying χ_{C18}. The surface coverage of C18 (χ^{σ}_{C18}), shown on the top of each image, was calculated from a model fit to ellipsometric measurements of the monolayer thickness (see main text). All scale bars are 100 μm.

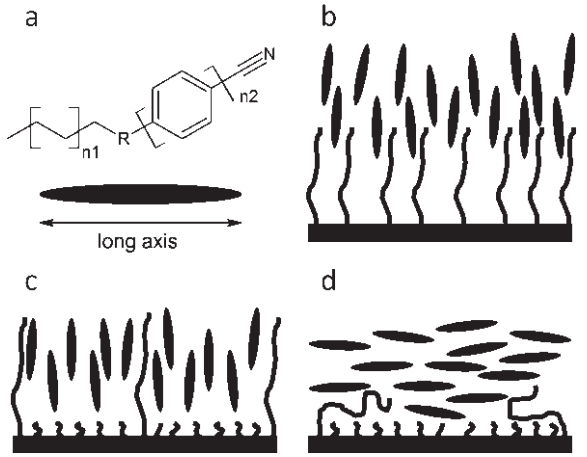

Figure 3. Mixed Monolayer Structure: (a) Molecular structure of the E7 mixture used with 51%: $n1 = 1$, R═C, $n2 = 2$; 25%: $n1 = 2$, R═C, $n2 = 2$; 16%: $n1 = 3$, R═O, $n2 = 2$; 8%: $n1 = 1$, R═C, $n2 = 3$; (b−d) Schematic illustration of the SAM−LC interface at different surface coverage of C18 (b) =1.0, (c) ≥0.11 (homeotropic), and (d) ≤0.05 (planar/tilted).

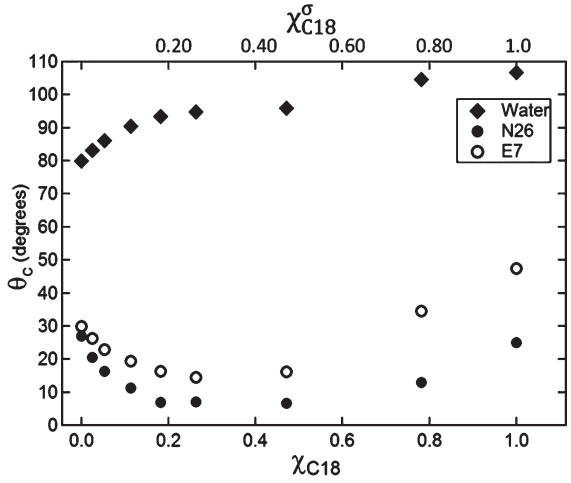

Figure 4. Contact Angle: The contact angle of several fluids on a C2/C18 mixed monolayer at varying χ_{C18}. The surface coverage of C18 (χ^{σ}_{C18}) shown on the top axis was calculated from a model fit to measurements of the monolayer thickness as described in the text. (Error bars are omitted as they are smaller than the size of the symbols used.)

differential apparent surface affinities of the C2 and C18 silanes. The mixed monolayer film thickness (h) is expressed as a weighted average based on the relative surface concentrations of C18 and C2 and the thicknesses of the pure C18 and C2 monolayers:

$$h = \frac{\chi_{C18}(h_{C18} - h_{C2})}{\chi_{C18}(1-n) + n} + h_{C2} \quad (1)$$

where h_{C18} is the thickness of a C18 monolayer, h_{C2} is the thickness of a C2 monolayer, and n is the ratio of the surface affinity of C2 to that of C18. The experimental data was fit to eq 1 (Figure 1a), and it was found that $n = 1.0 \pm 0.3$ (see Supporting Information for more details). Furthermore, an analytical equation for determining χ^{σ}_{C18} from χ_{C18} was obtained:

$$\chi^{\sigma}_{C18} = \frac{\chi_{C18}}{n(1-\chi_{C18}) + \chi_{C18}} \quad (2)$$

Figure 1b shows this dependence of χ^{σ}_{C18} on χ_{C18} illustrating that C2 becomes incorporated into the mixed SAM with the same apparent affinity as C18. The error in the measured values increases with increasing χ_{C18} due to the propagation of error completed in the calculation of χ^{σ}_{C18}.

RESULTS AND DISCUSSION

Liquid Crystal Anchoring on Mixed SAMs. Since surfaces functionalized with C2 and C18 SAMs induce planar and homeotropic LC anchoring, respectively,[32] and a similar long chain/short chain (i.e., DMOAP/MAP) mixed monolayer has been shown to decrease the planar anchoring strength with increasing DMOAP mole fraction,[33] we hypothesized that an LC anchoring transition would be observed as a function of χ_{C18}. This was indeed observed, as shown in Figure 2. Figures 2a and 2i show images consistent with the expected planar and homeotropic anchoring for C2 and C18 functionalized surfaces, respectively. Figure 2b−h shows the transition from tilted to homeotropic LC orientation with increasing χ_{C18}. The transition was found to occur between $\chi_{C18} = 0.05$ (where the anchoring was tilted) and $\chi_{C18} = 0.11$ where (weak) homeotropic orientation was observed.

The LC anchoring transition was observed to occur at a χ^{σ}_{C18} of long chain hydrocarbons well below complete coverage ($0.05 \pm 0.02 \leq \chi^{\sigma}_{C18} \leq 0.11 \pm 0.04$). While the precise mechanism of homeotropic alignment on surfaces treated with a long chain SAM is not known, previous reports suggest the importance of LC infiltration into the nm-scale SAM environment. For example, second harmonic generation studies on an 8CB film supported on a DMOAP functionalized surface demonstrated that LC molecules can infiltrate the fluid DMOAP monolayer environment.[34] Furthermore, LC alignment studies on a mixed monolayer of alkanethiols on gold demonstrated that homeotropic alignment was not induced by a purely long alkyl chain monolayer, while

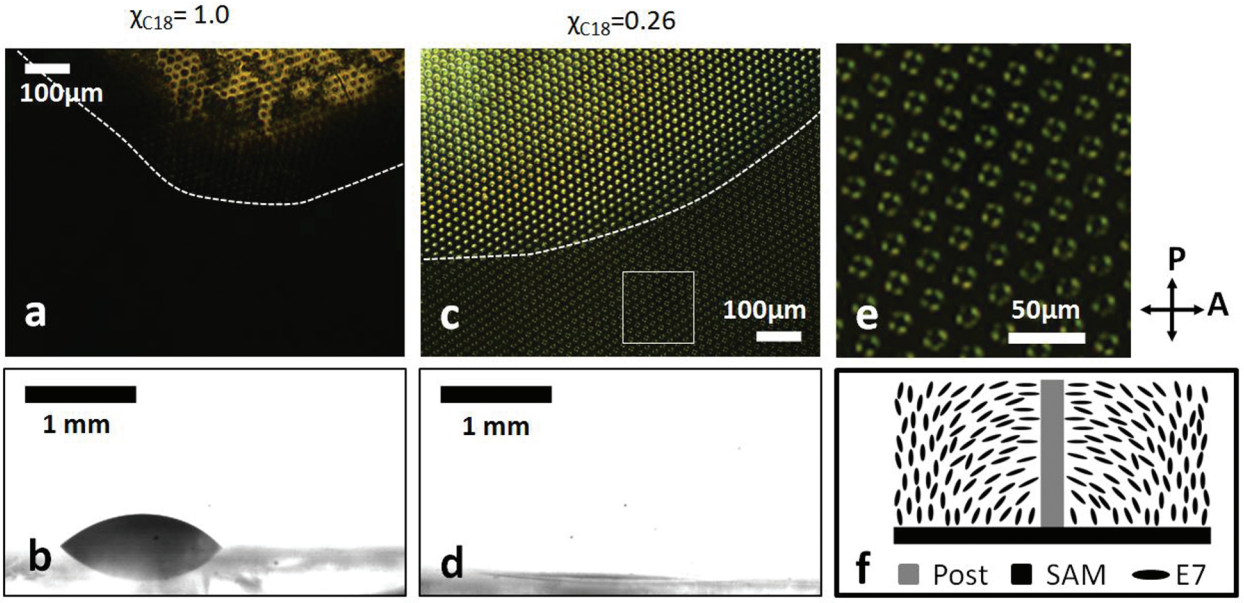

Figure 5. Sensor Wetting: LC droplets in contact with modified micropillar arrays. (a) Polarized light image (top-view) of a C18-functionalized array. The region above the dotted line shows the macroscopic LC droplet. (b) Side-view image of a C18-functionalized array. (c) Polarized light image (top-view) of a C18/C2-functionalized array (χ_{C18} = 0.26). The region above the dotted line shows the macroscopic LC droplet. (d) Side-view image of a C18/C2-modified array (χ_{C18} = 0.26). (e) The outlined region from part (c) enlarged 4.25× to illustrate the birefringence around the pillars and LC orientation in between the pillars. (f) A schematic illustrating the LC orientation when homeotropic orientation is induced on the SAM in between pillars (not to scale).

mixed monolayers did cause homeotropic alignment, a phenomenon partially attributed to the fluidity of the top layer of a mixed monolayer.[28] We speculate that similar behavior is observed in the mixed monolayers described here. At sufficiently high C18 coverage, the LC molecules infiltrate a fluid top layer and interact with the alkyl chains cooperatively so that the LC molecules as well as the alkyl chains align perpendicular to the interface (Figure 3b,c), resulting in homeotropic LC orientation. However, if the C18 surface coverage is too low, the long alkyl chains will lose their ordered structure and the LC orientation will be inhomogeneous, resulting in tilted/planar LC orientation (Figure 3d). This mechanism of LC orientation driven by steric interactions can be applied to a wide range of LC molecules (e.g., non-nitrile containing LC) as it is not limited to a specific coordination interaction as is the case with homeotropic alignment on surfaces functionalized with metal salts.

Contact Angles on Mixed SAMs. As expected, we found that increased presence of C18 at the interface resulted in systematically higher water contact angles as shown in Figure 4. Consistent with previous studies involving mixed monolayers of long and short chain alkylsilanes,[29,35−37] the contact angles of both organic liquids exhibited a nonmonotonic dependence of contact angle on C18 concentration. For example, as χ_{C18} (and therefore χ^{σ}_{C18}) decreased from unity (χ_{C18} = 1.0), the E7 contact angle (open circles in Figure 4) initially decreased from a maximum of 47.4 ± 0.5° to a minimum of 14.4 ± 0.1° at χ_{C18} = 0.26. At lower concentrations of C18, the LC contact angle gradually increased with a decrease in χ^{σ}_{C18} to 29.9 ± 0.5° for a pure C2 monolayer. The isotropic oil, N26, exhibited a similar nonmonotonic behavior (filled circles in Figure 4), suggesting that this behavior was not associated with the anisotropic physical properties of the LC. This is further supported by the observation that the composition corresponding to the contact angle minimum does not correspond to an LC anchoring transition, as observed not only for the C2/C18 mixed monolayer (above) but also for either a C1/C18 or C4/C18 mixed monolayer (see Supporting Information). These series of mixed monolayers composed of either C1/C18 or C4/C18 also demonstrated the same qualitative contact angle dependence on χ_{C18} for the isotropic oil and LC suggesting that, independent of mixed monolayer composition, the anisotropic contribution to the overall surface energy is a relatively small component. Studies have suggested that the nonmonotonic dependence of contact angle on coverage may be due to a varying coverage of surface methyl and methylene groups,[29,35−37] while the monotonic decrease observed for water is due to a relatively small difference between the water contact angle on purely methyl and methylene surfaces.[38]

Application to Micro-Structured Substrates. To explicitly demonstrate the ability of mixed monolayers to improve LC spreading and stability on microstructured substrates, a micropillar array was functionalized with a C18 SAM and a mixed C2/C18 SAM (χ_{C18} = 0.26). The LC wettability and the LC orientation were determined on these two substrates by measuring the LC contact angle and imaging the LC film between crossed polarizers. If the LC infiltrates the micropillar array, the relevant LC orientation at the SAM−LC interface can be determined by observing the light transmission in the regions between the micropillars, since the LC adopts a homeotropic orientation at the opposing air−LC interface.[39] However, the micropillar surface (which is modified by the silane deposition) induces homeotropic LC orientation relative to the micropillar surface (or planar relative to the specimen plane), as illustrated in Figure 5f. Therefore, birefringence is always observed around the edges of the micropillar if the LC is able to infiltrate the micropillar array, making the area around the micropillars visible

as small arcs when the sample is viewed between crossed polarizers.[5] However, if the LC does not infiltrate the micropillar array, the micropillars are not visible because they are surrounded by air, an isotropic medium. Thus, the presence of birefringent arcs is a signature characteristic of the presence of LC in the array.

We found that, for a micropillar array functionalized with a C18 monolayer, the LC did not infiltrate the array. Figure 5a shows a polarized microscopic image of a LC drop on the C18 functionalized array. In this image, the LC drop is visible as a semicircle at the top of the image (outlined by the area above the dashed line), demonstrating the expected birefringence due to the thickness and curvature of the LC drop, which covers the tops of the micropillars in this region. However, the micropillars outside of the LC drop are not visible, since the LC did not infiltrate the array. Furthermore, a relatively large contact angle on the micropillar array functionalized with pure C18 was directly observed as shown in Figure 5b. In this image, the micropillar array is to the right of the drop, and a monolayer on planar glass is to the left of the drop. It is seen that the contact angle on the micropillar array is similar to that on the glass, indicating that the interfacial energy causes the LC drop to bead on the array and prevents infiltration among the micropillars.

On the other hand, when the micropillar array was functionalized with an appropriate mixed C2/C18 SAM ($\chi_{C18} = 0.26$), the interfacial surface energy promotes low LC contact angle and spontaneous infiltration of LC among the micropillars. High birefringence was observed in the area occupied by the actual bulk LC drop (Figure 5c) since the drop covers the top of the micropillars (again, outlined by the area above the dashed line). In contrast to the array functionalized with the C18 monolayer, however, the micropillars outside the bulk LC drop were visible, surrounded by small arcs (Figure 5c,e), less bright than in the bulk LC drop, indicating that a thin LC layer successfully infiltrated the micropillar array. Homeotropic orientation was maintained in the areas between the micropillars as evidenced by the dark appearance of the area between the micropillars, in agreement with the observation in LC cells. Further verification that the LC infiltrated the micropillar array is shown in Figure 5d. A side view of the LC drop was captured on the mixed monolayer micropillar array. The interfacial energy promotes spontaneous spreading of the LC droplet with a very small contact angle that is difficult to measure, providing direct evidence for improved LC wetting in the post array.

CONCLUSIONS

Surface functionalization with a mixed monolayer composed of long and short chain alkylsilanes provided a robust strategy for controlling surface properties that are critical to LC sensor applications. The LC contact angle was reduced from 47.4° ± 0.5° on a purely C18 monolayer to 14.4° ± 0.1° when the surface coverage density drops to $\chi^{\sigma}_{C18} = 0.26$. Nonmonotonic behavior of the LC contact angle with respect to χ^{σ}_{C18} was observed and attributed to the isotropic contribution of the surface energy. A LC anchoring transition from planar to homeotropic LC orientation was observed for a C2/C18 mixed monolayer with $\chi^{\sigma}_{C18} \geq 0.11 \pm 0.04$, allowing for the design of a mixed monolayer that minimized the LC contact angle while maintaining homeotropic orientation. A surface functionalized with a mixed SAM was designed that allowed for homeotropic LC orientation with good LC wetting at $\chi^{\sigma}_{C18} = 0.26 \pm 0.09$ and was used to directly demonstrate the improved LC infiltration into a microstructured substrate illustrating the practical value of this approach.

ASSOCIATED CONTENT

Supporting Information. The derivation of a model to obtain the relationship between χ^{σ}_{C18} and χ_{C18} and the results for C1/C18 and C4/C18 mixed monolayers. This material is available free of charge via the Internet at http://pubs.acs.org.

AUTHOR INFORMATION

Corresponding Author
*E-mail: daniel.schwartz@colorado.edu.

ACKNOWLEDGMENT

This work was supported by the Liquid Crystal Materials Research Center (NSF/MRSEC, Award No. DMR-820579) and the Colorado State Bioscience Proof-of-Concept Grant (09BGF13).

REFERENCES

(1) Most, D. R.; Vantreeck, H. J.; Grinwald, B. A.; Kupcho, K. A.; Sen, A.; Bonds, M. D.; Anhalt, K.; Israel, B. A.; Acharya, B. R. *Proc. SPIE 7955, 79550L* **2011**, doi:10.1117/12.881429.
(2) Choi, Y. S.; Lee, Y. J.; Kwon, H. J.; Lee, S. D. *Mater. Sci. Eng., C* **2004**, *24*, 237–240.
(3) Price, A. D.; Schwartz, D. K. *J. Am. Chem. Soc.* **2008**, *130*, 8188–8194.
(4) Adgate, J. L.; Bartekova, A.; Raynor, P. C.; Griggs, J. G.; Ryan, A. D.; Acharya, B. R.; Volkmann, C. J.; Most, D. D.; Lai, S.; Bonds, M. D. *J. Environ. Monit.* **2009**, *11*, 49–55.
(5) VanTreek, H. J.; Most, D. R.; Grinwald, B. A.; Kupcho, K. A.; Bonds, M. D.; Acharya, B. R. *Sens. Actuators, B* **2011**, *158*, 104–110.
(6) Bi, X. Y.; Yang, K. L. *Sens. Actuators, B* **2008**, *134*, 432–437.
(7) Brake, J. M.; Daschner, M. K.; Luk, Y. Y.; Abbott, N. L. *Science* **2003**, *302*, 2094–2097.
(8) Brake, J. M.; Abbott, N. L. *Langmuir* **2002**, *18*, 6101–6109.
(9) Cheng, D. M.; Sridharamurthy, S. S.; Hunter, J. T.; Park, J. S.; Abbott, N. L.; Jiang, H. R. *J. Microelectromech. Syst.* **2009**, *18*, 973–982.
(10) Evans, S. D.; Allinson, H.; Boden, N.; Henderson, J. R. *Faraday Discuss.* **1996**, 37–48.
(11) Kahn, F. J.; Taylor, G. N.; Schonhor., H *Proc. IEEE* **1973**, *61*, 823–828.
(12) Kubono, A.; Onoda, H.; Inoue, K.; Tanaka, K.; Akiyama, R. *Mol. Cryst. Liq. Cryst.* **2002**, *373*, 127–141.
(13) Walba, D. M.; Liberko, C. A.; Korblova, E.; Farrow, M.; Furtak, T. E.; Chow, B. C.; Schwartz, D. K.; Freeman, A. S.; Douglas, K.; Williams, S. D.; Klittnick, A. F.; Clark, N. A. *Liq. Cryst.* **2004**, *31*, 481–489.
(14) Zhang, J.; Hoogboom, J.; Kouwer, P. H. J.; Rowan, A. E.; Rasing, T. *J. Phys. Chem. C* **2008**, *112*, 20105–20108.
(15) Bi, X. Y.; Yang, K. L. *J. Phys. Chem. C* **2008**, *112*, 1748–1750.
(16) Doudevski, I.; Hayes, W. A.; Schwartz, D. K. *Phys. Rev. Lett.* **1998**, *81*, 4927–4930.
(17) Leitner, T.; Friedbacher, G.; Vallant, T.; Brunner, H.; Mayer, U.; Hoffmann, H. *Mikrochim. Acta* **2000**, *133*, 331–336.
(18) Wang, Y. L.; Lieberman, M. *Langmuir* **2003**, *19*, 1159–1167.
(19) Fadeev, A. Y.; McCarthy, T. J. *Langmuir* **2000**, *16*, 7268–7274.
(20) Haller, I. *Appl. Phys. Lett.* **1974**, *24*, 349–351.
(21) Naemura, S. *J. Appl. Phys.* **1980**, *51*, 6149–6159.
(22) Nakano, F.; Isogai, M.; Yokokura, H. *Jpn. J. Appl. Phys.* **1995**, *34*, 5736–5737.
(23) Sen, A. S. A.; Acharya, B. R. *Liq. Cryst.* **2011**, *38*, 495–506.

(24) Lee, S. H.; Lin, W. C.; Kuo, C. H.; Karakachian, M.; Lin, Y. C.; Yu, B. Y.; Shyue, J. J. *J. Phys. Chem. C* **2010**, *114*, 10512–10519.
(25) Lee, J. W.; Kim, H. T.; Sung, S. J.; Park, J. K. *Synth. Met.* **2001**, *117*, 267–269.
(26) Oh, S. K.; Nakagawa, M.; Ichimura, K. *J. Mater. Chem.* **2001**, *11*, 1563–1569.
(27) Gupta, J. K.; Abbott, N. L. *Langmuir* **2009**, *25*, 2026–2033.
(28) Drawhorn, R. A.; Abbott, N. L. *J. Phys. Chem.* **1995**, *99*, 16511–16515.
(29) Vilt, S. G.; Leng, Z. W.; Booth, B. D.; McCabe, C.; Jennings, G. K. *J. Phys. Chem. C* **2009**, *113*, 14972–14977.
(30) Sugimura, H.; Hozumi, A.; Kameyama, T.; Takai, O. *Surf. Interface Anal.* **2002**, *34*, 550–554.
(31) Depalma, V.; Tillman, N. *Langmuir* **1989**, *5*, 868–872.
(32) Malone, S. M.; Schwartz, D. K. *Langmuir* **2008**, *24*, 9790–9794.
(33) Guo, W.; Bahr, C. *Phys. Rev. E* **2009**, 79.
(34) Huang, J. Y.; Superfine, R.; Shen, Y. R. *Phys. Rev. A: At., Mol., Opt. Phys.* **1990**, *42*, 3660–3663.
(35) Laibinis, P. E.; Nuzzo, R. G.; Whitesides, G. M. *J. Phys. Chem.* **1992**, *96*, 5097–5105.
(36) Zhang, Q.; Archer, L. A. *J. Phys. Chem. B* **2003**, *107*, 13123–13132.
(37) Zhang, Q.; Archer, L. A. *Langmuir* **2005**, *21*, 5405–5413.
(38) Adam, N. K.; Elliott, G. E. P. *J. Chem. Soc* **1962**, 2206–2209.
(39) Nazarenko, V.; Nych, A. *Phys. Rev. E: Stat., Nonlinear, Soft Matter Phys.* **1999**, *60*, R3495–R3497.